Reappraisal of Upscaling Descriptors for Transient Two-Phase Flows in Fibrous Media

Aubin Geoffre, Nicolas Moulin, Julien Bruchon, Sylvain Drapier

Reappraisal of upscaling descriptors for transient two-phase flows in fibrous media

Aubin Geoffre[1*], Nicolas Moulin[1†], Julien Bruchon[1†] and Sylvain Drapier[1†]

[1*]Hexcel Industrial Chair - Mines Saint-Étienne, Université de Lyon, CNRS, UMR 5307 LGF, Centre SMS, 158 Cours Fauriel, Saint-Étienne, 42023, France.

*Corresponding author(s). E-mail(s): a.geoffre@emse.fr; Contributing authors: nmoulin@emse.fr; bruchon@emse.fr; drapier@emse.fr;

†These authors contributed equally to this work.

Abstract

Transient two-phase flows within fibrous media are considered at local scale. Upscaling these flows constitute a key procedure towards a tractable description in an industrial context. However, the task remains challenging as a time-dependent behaviour is observed within a geometrically complex structure with interplay of various physical phenomena (capillary effects, viscous dissipation,...). The usual upscaling strategies, encountered in both soil sciences and composite materials communities are reviewed, compared, and finally adapted to reach a method that is relevant to describe fibrous media imbibition. Using finite element flow simulations on statistical representative volume elements, the proposed approach first considers several definitions for saturation in order to characterise the flow dynamics as well as the characteristic length associated with the transient behaviour. Next, two methods are proposed to assess a resulting capillary pressure, demonstrating the importance to properly define the capillary pressure acting on the interface. The first one considers the mean pressure jump at the interface while the second one uses a machine-learning technique, namely Gaussian Process Regression, to retrieve the mean curvature of the interface. Those methods are found to be both consistent and in agreement with the results from the literature.

Finally, a novel approach that stochastically describes the position of the flow front through a presence distribution is detailed. The spread of the front can be compared to the saturation length and its value has been found to be small enough to be neglected at upper scale, justifying the use of sharp interface models for similar porous media and flow settings.

Keywords: Upscaling, Capillary pressure, Two-phase flow simulations, Gaussian Process Regression

Notations and abbreviations (text order)

RVE	Representative Volume Element
S_L	Liquid saturation of the volume
S_L^{max}	Maximum liquid saturation of the volume
t	Time variable
Ca	Capillary number
η_i	Viscosity of phase i
v_{in}	Inlet velocity
γ_j	Surface tension coefficient of interface j
P^c_{vol}	Resulting capillary pressure (volume definition)
p	Fluid pressure field
$\langle\cdot\rangle^i$	Volume averaging operator over phase i
Ω_i	Domain associated with phase i
$\lvert\omega\rvert$	Volume/surface of domain ω
$P^c_{vol,dyn}$	Dynamic capillary pressure (volume definition)
τ	Relaxation coefficient associated with $P^c_{vol,dyn}$
$[\![p]\!]_j$	Pressure jump at interface Γ_j
$\mathscr{C}$	Mean curvature
$\langle\rangle^{LV}$	Surface averaging operator over the liquid-vapor interface Γ_{LV}

P_p^c	Resulting capillary pressure (pressure jump definition)
P_C^c	Resulting capillary pressure (mean curvature definition)
Ω	Computational domain
ρ_i	Density of phase i
$\bar{r}$	Average fibre radius
$\boldsymbol{v}$	Fluid velocity field
ϕ	Level-set field
ASGS	Algebraic SubGrid Scale
SUPG	Streamline Upwind Petrov-Galerkin
V_f	Fibre volume ratio
SRVE	Statistical Representative Volume Element
L	Characteristic length of the computational domain
$s_L(A)$	Liquid saturation of section A
$s_L^{max}(A)$	Maximum liquid saturation of section A
R	Ratio between $s_L(A)$ and $s_L^{max}(A)$
ℓ_s	Saturation length
GPR	Gaussian Process Regression
$\mathscr{F}$	Area containing the flow front
$\boldsymbol{x}_i^{\mathscr{F}}$	Coordinates of the vertices that shape the flow front
$I_{\boldsymbol{x}_{\mathscr{F}}}$	Random variable which realisations give $\boldsymbol{x}_i^{\mathscr{F}}$
ℓ_s^*	Saturation length averaged over time
P_p^{c*}	Asymptotic value of P_p^c
P_C^{c*}	Asymptotic value of P_C^c
μ	Mean value of the flow front distribution
σ	Standard deviation of the flow front
σ^*	Asymptotic value of σ

1 Introduction

Multiphase flows in fibrous media are commonly observed in numerous fields going from soil science [1–3] to composite manufacturing processes [4, 5] where a carbon fibre preform that initially contains rarefied air is filled with a liquid resin. A multiphase flow resin/air within a porous fibrous medium is thus observed. This medium naturally shows several scales of description, starting from the scale of the carbon fibre ($\sim \mu$m) to the scale of the industrial part ($\sim$ m). As flow models must be adapted to the scale of representation, connecting those microscopic and macroscopic scales has been a major concern in the scientific community. As a first approach, a permeability tensor that represents the ability of the fibrous structure to be crossed by a fluid is generally studied. This concept has been first introduced following Darcy's works to macroscopically describe a monophasic steady flow in a porous medium [6]. Besides, the complexity of a multiphase flow can hardly be reduced to a single tensor. Such flows are indeed considerably more challenging to describe as several phases are observed with a moving interface. The observed behaviour becomes non-linear, time-dependent and sensitive to many parameters such as fluid properties or boundary conditions. In addition to this, the vicinity between carbon fibres, around few micrometers, leads to consider capillary effects and consequently a sentivity to surface tension coefficients [7, 8].

From early theoretical works, upscaling strategies from Representative Volume Elements (RVE) have been proposed to transpose the microscopic description of multiphase flows in porous media towards an upper scale [3, 9–11]. Those have been mainly developed by the hydrogeology community for the study of flows within soils or rocks. Later on, the composite materials community have developed its own approaches, that are particularly suited for the study of fibrous materials impregnation but that may suffer from a lack of sound theoretical ground. The novelty of this contribution consists in operating an explicit connection between both types of approaches, so as to retrieve a rigourous, precise, and complete description that is adapted to the imbibition of fibrous media while carrying the specificities and constraints inherent to composite materials.

1.1 Saturation

The most straighforward upscaling quantity is the liquid saturation $S_L \in [0, 1]$ that describes the proportion of liquid within the poral space. As imbibition is considered here, S_L increases over time from 0 to a maximal value $S_L^{max} = S_L(t \to \infty)$ obtained when the two-phase flow reaches steadiness. The relation $S_L = S_L(t)$ characterises the global dynamics of the flow. The asymptotic saturation value S_L^{max} is lower than 1 as the flow tends to entrap air bubbles behind the front. This proportion of residual phase at final state is a concern in many fields since it can be associated with a recovery ratio in hydrology [12] or a void content in the composite materials community [13]. As bubble entrapment phenomenon results from velocity inhomogeneity over the volume, S_L^{max} value is expected to be directly dependent on the competition between viscous and capillary effects. This is expressed through the capillary number Ca that is defined here as:

$$Ca = \frac{\eta_L v_{in}}{\gamma_{LV}} \tag{1}$$

where η_L is the liquid viscosity, v_{in} the inlet velocity and γ_{LV} the surface tension coefficient from the liquid-vapor interface.

Studying the saturation finally describes a complex phenomenon through a single time-dependent scalar. It is especially convenient at upper scales where the two-phase flow can be modeled as a transport of saturation in an equivalent homogeneous medium [14]. However, in the context of an upscaling procedure, a global saturation only provides a rough description of the flow without spatial information. As a consequence, a first improvement consists in defining saturation at a more local scale. This is observed in the literature related to composite materials processes where local saturation curves are often considered [15–19], they consist in representing saturation as a function of position at a given time. A transition between two saturation regimes is observed, its characteristic width is referred to as *saturation length*. This approach is particularly suited for the type of flow and geometry under consideration, that is to say the impregnation of fibrous reinforcements as encountered in aeronautical structural applications and that locally show a statistically homogeneous nature. It thus may be complex to transpose to other specific contexts, like wicking in 3D structures, where further difficulties arise, such as pore delays [20].

1.2 Capillary effects

Capillary effects rising from surface tension phenomena act as a complementary force in the filling of fibrous microstructures. However, in a more general context, it depends on the fluids under consideration as well as the pore structure. In the context of manufacturing processes of composite materials, it is generally considered as a driving force that helps the impregnation [7]. In any case, this contribution has to be upscaled. This is achieved through the introduction of a *resulting* capillary pressure P^c. Though the *capillary pressure* term is widely encountered in literature, it may admit several definitions and approaches. In literature and especially in the hydrogeology community, it is generally defined at the volume scale [21]. A first definition P^c_{vol} is thus obtained as the difference between volume-averaged phase pressure:

$$P^c_{vol} = \langle p_V \rangle^V - \langle p_L \rangle^L \tag{2}$$

where p_i is the pressure field associated to phase i. From now on, L will refer to the liquid phase, V to the vapor phase and S to the solid one. Such a definition (Eq.2) requires volume-averaging operator:

$$\langle \cdot \rangle^i = \frac{1}{|\Omega_i|} \int_{\Omega_i} \cdot \, dV \tag{3}$$

Those volume-defined capillary pressures are generally expressed as a function of the saturation S_L [22]. The determination of capillary pressure-saturation curves constitutes a huge area of research as they are considered to characterise the two-phase flow at a macroscopic level. They finally provide a simple macroscopic relation that is convenient to use in practice especially when transport of saturation is considered.

However, obtaining capillary pressure-saturation curves is challenging for several reasons. First, an hysterisis phenomenon is classicaly observed between the imbibition and drainage curves [23]. Besides, it has been shown that equilibrium must be reached so that Eq.2 match the capillary pressure [24, 25]. This especially makes the experimental determination of $P^c_{vol} - S_L$ curves very time-consuming since for a given saturation value, the flow may take several hours to stabilise towards a steady state [26]. In parallel, flows observed in practice generally show a transient behaviour where the static equilibrium is never met. This finally leads to consider *dynamic capillary effects* for which a considerable amount of contribution can be found [23, 27, 28]. In the context of these works, the instantaneous difference of phase pressure $P^c_{vol,dyn}$ is then measured and related to the static pressure through the (de)saturation rate

[21]:

$$P^c_{vol,dyn} = P^c_{vol} - \tau \frac{\partial S_L}{\partial t} \quad (4)$$

where the dynamic coefficient τ controls the rate to reach the equilibrium. The value for this coefficient can span several orders of magnitude and its dependancies are complex and still on study [23, 27–30]. It should be noticed that $P^c_{vol,dyn}$ is sometimes referred to as *dynamic capillary pressure* which is somehow ambiguous as the quantity does not rely on any rigourous justification based on capillary laws.

1.3 Interfacial capillary pressure

In spite of its apparent simplicity and the convenience of its use, a capillary pressure-saturation relationship can finally be complex to determine and raise numerous modelling questions. More generally, assuming that capillary effects match a global difference between phase pressures is not straightforward [31]. Mathematically, capillary action is taken into account through the Laplace's law (Eq.5) that only holds at the interface between two phases:

$$[\![p]\!]_j = \gamma_j \mathscr{C} \quad \text{in} \quad \Gamma_j(t) \quad (5)$$

where $[\![p]\!]_j$ is the pressure field discontinuity at interface Γ_j, characterised by its surface tension γ_j and by a mean curvature $\mathscr{C}$.

As a consequence, a rigourous upscaling procedure cannot retrieve a volume definition of capillary pressure. All these arguments lead to reavalute the common volume definition of capillary pressure. To be consistent with the physics of the problem, as well as the upscaling procedure, a resulting capillary pressure computed at the interface level should be considered [25, 32]. Starting from Eq.5, a surface averaging over the liquid-vapor interface can be carried out through an operator $\langle\cdot\rangle^{LV}$:

$$\langle\cdot\rangle^{LV} = \frac{1}{|\Gamma_{LV}|}\int_{\Gamma_{LV}} \cdot\, dS \tag{6}$$

This gives two other approaches for considering resulting capillary pressure. A first one consists in averaging the pressure jump [33, 34] while the second integrates the mean curvature over the interface [11, 24, 34, 35]:

$$P^c_p = \langle [\![p]\!]_{LV}\rangle^{LV} \tag{7}$$

$$P^c_{\mathscr{C}} = \gamma_{LV}\langle\mathscr{C}\rangle^{LV} \tag{8}$$

As capillary pressure becomes defined at interface level, its dependancies to time or saturation can be reappraised. Indeed, capillary pressure does not correspond anymore to a volume scale driving force that may depend on the proportion of each phase. Instead, the resulting capillary action can be expected to be only a function of the porous geometry and surface tension coefficients. This is in agreement with the composite materials literature [7, 36] in which capillary pressure is considered as an intrinsic property of the porous medium and fluids.

1.4 Description of the flow front

Finally, a novel method to characterise the flow front is proposed in this work. As the flow front is fragmented and discontinuous within the complex poral structure, modeling it in a deterministic way may be criticised [19]. Consequently, a statistical modelling is proposed where the flow front is characterised by a presence distribution. At an upper scale, this allows us to assess the mean position of the flow front as well as its spread across the poral structure, which is particularly relevant in the study of complex porous media.

This paper will first recall the numerical strategy for the simulation of transient two-phase flow (Section 2.1). Next, the proposed upscaling procedure will be detailed (Section 2.2). Then the results will be presented (Section 3) and discussed (Section 4).

2 Materials and methods

The physical modelling of transient two-phase flow is now detailed. Such a problem is solved within a stabilised finite element framework that has been presented in previous studies and that will be briefly recalled here. Particuliar attention is paid to the generation method of fibrous geometries and to boundary conditions. Then the proposed upscaling method will be explained.

2.1 Numerical simulation of a two-phase flow within a fibrous medium

2.1.1 Physical problem and conservation laws

Two-phase flows with a moving interface are here adressed by solving two coupled problems. The first one corresponds to the fluid problem and consists in solving mass and momentum conservation equations on the computational domain Ω (Fig.1). Both liquid and vapor phases are assumed to be newtonian fluids and the flow incompressible. As the invading phase under consideration shows a high viscosity and low velocity, a sufficiently low Reynolds number can be assumed:

$$Re = \frac{2\bar{r}\rho_L v_{in}}{\eta_L} \ll 1 \tag{9}$$

where ρ_L is the liquid density and $\bar{r}$ the average fibre radius. Consequently, the convective and transient terms of Navier-Stokes' equations can be discarded. As a consequence, Stokes equations are here considered [37]. Let us consider that phase $i \in \{L, V\}$ occupies a domain $\Omega_i(t)$ at time t. The following problem is solved:

$$\left.\begin{aligned} \boldsymbol{\nabla} \cdot \boldsymbol{v} &= 0 \\ \eta_i \boldsymbol{\Delta} \boldsymbol{v} - \boldsymbol{\nabla} p &= 0 \end{aligned}\right\} \quad \text{in} \quad \Omega_i(t) \tag{10}$$

As an interface condition, no-slip is prescribed on the fibres.

Capillary effects are taken into account through Laplace's relationship already introduced in Eq.5 where $j \in \{LV, LS, SL\}$ (Fig.1). The contributions associated to the solid phase in Eq.5 vanish, as the fibres are supposed to be non-deformable. As a numerical consequence, the solid domain Ω_S is not meshed. Surface tension coefficients and viscosities are chosen to be consistent with experimental measurements [38] encountered in direct manufacturing processes of composite materials, and can be found in Table 1.

The model requires to locate the phases and the liquid-vapor interface Γ_{LV} in order to compute capillary terms or to apply the proper fluid properties. The interface is here modeled implicitly with a level-set method. The method leans on a scalar field ϕ that describes the signed distance between each point of the computational domain and the liquid-vapor interface [39]. Therefore the zero iso-value of the field correponds to the liquid-vapor interface. The whole field is then convected in the fluid velocity field $\boldsymbol{v}$ to describe the moving interface [37]:

$$\frac{\partial \phi}{\partial t} + \boldsymbol{v} \cdot \boldsymbol{\nabla} \phi = 0 \quad \text{in} \quad \Omega \tag{11}$$

with $\Omega = \Omega_L \cup \Omega_V$. The resolution of Eq.11 requires both initial and boundary conditions. The initial level-set field corresponds to a plane liquid/vapor interface, close to the inlet boundary. A boundary condition, usually on the inlet boundary, is prescribed as a non-zero constant value for which the sign indicates which phase enters the volume. Finally, to ensure that the field ϕ remains a distance function throughout the computation, a reinitilisation step is performed [40, 41].

2.1.2 Numerical strategy for solving the physical problem

The problem described in the previous section (Eqs. 10,11) is solved with a finite element approach through an in-house implementation in Z-set software[1]. The validity of the numerical strategy has been proved in various contributions [37, 42–48]. The fluid problem is solved using linear approximations for both velocity and pressure fields, associated with an ASGS strategy [49, 50]. The implementation of capillary conditions at interfaces will not be detailed here but further explanations can be found in [43]. Then, the level-set field is also approximated by linear functions and its convection (Eq.11) is stabilised by a SUPG method [51]. Both fluid and level-set problems share the same mesh and are weakly coupled. An exemple of simulation within a fibrous microstructure is represented in Fig.2.

2.1.3 Generation of fibrous microstructures

The porous medium under consideration is made of long carbon fibres. As a consequence, it is common to work within the plane that is tranverse to the fibre axis [46]. This leads us to consider a 2D flow around a set of disks.

Fibrous microstructures have thus been randomly generated, from an input value of fibre volume ratio V_f, and through an algorithm detailed in a previous contribution [46]. In that paper, it was shown that the generated microstructures are statistically representative of real fibrous structures with respect

[1] http://www.zset-software.com/

to both mechanical response and geometrical considerations. In that sense, the microstructures can be considered as Statistical Representative Volume Elements (SRVE) [52]. The geometries are thus able to grasp the inherent randomness of the medium. To our knowledge, studying the impregnation of fibrous media from such volumes through transient two-phase flow simulations is a novelty, as similar studies are generally based on idealised representations of fibrous structures, using unit cells for instance.

In [46], a (S)RVE size has been determined for permeability considering steady flow simulations. It has been remarked that RVE is met for a size L such that $L/\bar{r} \approx 80$. However, for significantly lower value of $L/\bar{r}$, the results have been found to yield permeabilities very close to the asymptotic value. As a result, the RVE size has been set at 50 as a satisfactory trade-off between the statistical representativity and the computation cost. Fibre density will be kept here at 50% to consider an intermediate value.

2.2 Upscaling methods

2.2.1 Saturation

Saturation S_L is defined here as the proportion of liquid volume $|\Omega_L|$ over the overall poral volume $|\Omega|$:

$$S_L = \frac{|\Omega_L|}{|\Omega|} \tag{12}$$

It is thus defined at the volume scale and gives a global characterisation of the flow. Its temporal evolution translates the overall dynamics of the flow. It especially depends on the flow control that is prescribed through inlet/outlet boundaries of the volume (Fig.3). The imbibition of the fibrous structure is mainly driven by the boundary conditions prescribed at the inlet/outlet boundaries. Depending on whether a pressure drop or a flow rate is prescribed, the dynamics of impregnation can be significantly different. Consequently, as discussed in the next paragraph, the type of flow control influences direclty the time evolution of S_L.

When the same constant flow rate is prescribed at the inlet/outlet boundaries, the time evolution of S_L is first linear as the incompressible fluid is forced to travel the same distance at any time (Fig.3). Then, saturation converges towards an asymptotic value S_L^{max} as the flow reaches steadiness. On the contrary, if a pressure drop between the inlet and oulet boundaries is prescribed, the time evolution of S_L is non-linear and a clear transition between flow regimes is complex to identify. As the liquid fills the pore space, the overall volume viscosity increases and the fluid displacement induced by the pressure drop becomes increasingly smaller. Consequently, the average fluid velocity may drop by several orders magnitude between the beginning and the end of the simulation. This may alter the flow behaviour over time, particularly the competition between viscous and capillary effects which is represented through the capillary number Ca [53] (Eq.1).

In infusion-based manufacturing processes for composite materials, a pressure drop is imposed at the industrial part scale. At the local scale under consideration, this would lead to prescribe different pressure values on opposite sides of the domain. However, the aim of this study is to characterise the upscaling of local flows. For this purpose, it seems necessary to have a strong control on the flow regime throughout the simulation: a flow rate control will be prescribed on the volume in the rest of the study. A wall condition (i.e. $\boldsymbol{v} = \mathbf{0}$) is applied on the boundaries that are parallel to the imposed flow. Note that, although the microstructure is periodic, no periodic boundary condition has been used here. Indeed, in the case of a two-phase flow a periodic boundary condition should ensure the periodicity of the velocity, but should also guarantee that the same phase is considered on the corresponding nodes of both boundaries.

Since the mechanical response is supposed to be independent of such boundary conditions as soon as the geometry can be regarded as a RVE, which is the case here [46], wall conditions have been considered throughout this study.

The slope of the $S_L = S_L(t)$ curve, as well as S_L^{max}, provide a global yet rough description of the flow. The characterisation can be carried further by giving a more localised definition. Let us consider a section A of surface $|A|$ whose normal vector is along the imposed flow-rate (Fig.4). At a given time t, this section contains a liquid surface $|A_L|$. This allows to define a local saturation $s_L(A)$ associated with section A as:

$$s_L(A) = \frac{|A_L|}{|A|} \tag{13}$$

This provides a time characterisation of the flow that also depends on the position. The $s_L(A)$ values are expected to be zero as long as the flow does not reach the section under consideration. Then a transition until a maximum value $s_L^{max}(A)$ should occur [18]. This value allows to characterise the steady flow that sets in section A. The transition time between the transient and steady states thus give an information about the local dynamics of the flow. However, it is more suitable to deal with a space variable as retrieving a physical time from numerical simulation of two-phase flow can be difficult [43, 54]. In the literature, local saturation is expressed as a function of the position considering that each section reaches full saturation. This asumption does not hold here as the void content at final state is not necessarily negligible. This leads to introduce the following quantity R:

$$R(t;\ A) = \frac{s_L(t;\ A)}{s_L^{max}(A)} \tag{14}$$

It describes, at time t and for a given section A, how reached the steady state is. As a consequence, $R = 0$ indicates that the fluid has not reached the section A yet. Inversely, the value $R = 1$ means that the flow is steady. For any value between 0 and 1, the flow is considered as transient. The value of R can be represented at a given time t as a function of the section position. Assuming an imbitition from the left side to the right one as depicted in Fig.4, $R(A;\ t)$ is expected to go from 1 to 0. The transition zone between those asymptotic values is associated to a *saturation length* ℓ_s corresponding to partially saturated zone. As the poral structure is isotropic, we expect this saturation length to stabilise towards a constant value. Even if the volume does not reach the rigorous RVE size, ℓ_s should be compared to the domain characteristic length so as to give first conclusions about the separation of scales.

2.2.2 Resulting capillary pressure

The resulting capillary pressure is here computed at the interface level from Eqs. 7 and 8. The methods to evaluate these quantity in practice are now detailed. An expression for the macroscopic capillary pressure is first obtained from the average pressure jump at the interface (Eq.7). To do so, elements of the mesh that are cut by the interface (i.e. the zero iso-value of the ϕ field) are scanned. For each one, the difference of mean pressure on either side of the interface is computed. This gives a distribution of local capillary pressure from which the median value is taken. This quantity will be referred to as *pressure jump* capillary pressure and denoted as P_p^c.

A second possibility to compute the capillary pressure is to consider the average mean curvature (Eq.8). Such an approach is usually avoided as it requires a double derivative computation which is numerically sensitive. As the liquid-vapor interface is generally non-continuous and fragmented, one must first isolate each continuous piece of Γ_{LV}. Considering the linear approximation of the fields, every interface piece corresponds to a small set of continuous segments which have first to be smoothened so that the mean curvature can be computed.

As a method suitable for small dataset while providing a good smoothing of the curves, a Gaussian Process Regression (GPR) technique is here selected [46, 55, 56]. Here, each continuous piece of interface is seen as a parametric curve. For each one, a GPR is carried out with the arc length as input and each cartesian coordinates as outputs. Then the mean curvature can be easily computed for each continous piece of the interface. This yields a distribution of mean curvature from which the median value is taken to retrieve a representative scalar quantity. This will be referred to as *mean curvature* capillary pressure and denoted as P_C^c. Despite the efficiency of the method, a considerable number of GPRs is required leading to significant computational costs.

Those methods for computing the interfacial capillary pressure are validated with the following test case: a 2D bubble with a unitary radius (i.e. a unitary curvature) is placed in a square domain (Fig.5). As a unitary surface tension coefficient is chosen, the capillary pressure is expected to be equal to one. In addition, a very low pressure drop is prescribed on the volume to make the bubble move slighly on the fixed mesh (Fig.5). As the pressure drop has a low intensity, no geometrical change of the bubble is observed and a simple translation occurs. This aims at assessing the robustness of the methods throughout the simulation.

The results of both methods are compared in Fig.6 for a given mesh. The relative error with respect to the expected unitary capillary pressure is plotted.

As for all the presented graphs, time t is normalised by the final time t_f. Even though both curves show a certain variability, it lies under 1% in absolute value. Furthermore, the median error for both capillary pressures gives very satisfactory results. The mesh convergence has also been studied as represented in Fig.7. As expected, the finer the mesh, the smaller the error. It should be remarked that mean curvature capillary pressure gives more precise results for a given mesh. The technique is especially very performing for coarse meshes. As regards the pressure jump capillary pressure, the precision of the method is enhanced by the enrichement of the elements cut by interface [43, 57]. Finally, both methods quickly converge towards the expected theoretical value. This gives us confidence in both of the proposed approaches.

2.2.3 Statistical description of the flow front

A new method to define the flow front position in the homogenised equivalent representation is now detailed. The main idea is to assume that the transient behaviour is only localised in a band, the characteristic length of which corresponds to the flow front width, as depicted in Fig.8. Outside this area, the behaviour is assumed to be steady. Indeed, a static equilibrium between phases is supposed to be met upstream while the fluid have not reached the downstream area yet. Inside $\mathscr{F}$ (Fig.8), the liquid-vapor interface is generally non-continuous. The presented approach considers the position of the interface within $\mathscr{F}$ through a statistical description. Considering our numerical approach, the interface corresponds to a set of segments for which endpoints position are denoted as $\boldsymbol{x}_i^{\mathscr{F}} = (x_i^{\mathscr{F}}, y_i^{\mathscr{F}})$. The coordinate that follows the flow direction is considered as a realisation of a random variable. In the example described in Fig.8, this corresponds to the abscissa of the points that compose the interface and it is denoted as $I_{x^{\mathscr{F}}}$. This random variable is expected to follow a Gaussian law, as the interface is mainly centred around a certain position and its density then decays symmetrically from it.

This method requires the identification of the flow front which can be difficult in practice. Here, the domain is divided into rectangles in the direction of flow (Fig.9). For each rectangle, the most downstream point of the interface is fetched ($\boldsymbol{x}^*$ for the dark blue rectangle in Fig.9) and its associated piece of interface is retrieved (the green piece of interface in Fig.9). This method allows a good reconstruction of the interface even if some errors of attribution may occur (Fig.10).

3 Results

Results obtained through the methods detailed previously are now presented. Transient two-phase flow simulations have been carried out in a numerically generated fibrous microstructure with a fibre density V_f equal to 50% and a capillary number Ca equal to 10^{-3}. This value is frequently chosen in the composite materials community as it has been shown to minimise the vapor content at final state, optimising therefore the impregnation quality [58, 59].

3.1 Global and local saturations

The global saturation S_L is first considered. An example of temporal evolution for S_L has been represented in Fig.11. As noticed previously, such a curve shows two regimes: a linear transient phase and a subsequent convergence towards a two-phase equilibrium as the liquid has filled-in the volume. Despite the simplicity of this behaviour, several upscaling descriptors with physical meaning can be extracted. The slope of the first phase can be computed to characterise the global dynamics of the flow. Then, the time to reach stability may be compared between different microstructures with the same fibre density and simulation parameters. At last, the asymptotic saturation value S_L^{max} corresponds to the residual proportion of vapor phase which is usually referred to as a void content in the composite materials community. Due to the flow incompressibility hypothesis, S_L^{max} may overestimate the experimentally observed values as density inside bubbles cannot change. These three descriptors (i.e. saturation curve slope, filling time and maximum saturation) will be studied more precisely through a statistical further study.

Saturation defined at section level is now under consideration. It can be first represented as a function of time for different sections of a same geometry. The observed behaviour follows the expected sigmoid as represented in Fig.12 for three given sections. As noticed previously, it is suitable to transpose the curve into the spatial domain to retrieve a saturation length. This has been achieved by considering the ratio R introduced in Section 2.2.1 as depicted in Fig.13 at three given times. From the transition width of these curves, saturation length ℓ_s can be derived at any given time. As a consequence, it can be considered as time-dependent as depicted in Fig.14. To recover a representative scalar quantity, saturation length is considered to be globally stable around a finite value ℓ_s^*, represented by a dashed line in Fig.14. In the case under consideration, this saturation length value is found to be around $7.6\bar{r}$. This means that the RVE size is sufficient here for the flow to settle in steady regime.

3.2 Resulting capillary pressure

The resulting capillary pressure is computed throughout the simulation duration. Both methods that have been presented previously are considered. The temporal evolution of P_p^c and P_C^c is represented in Fig.15.

It can be observed that both behaviours are in very close agreement. The curves eventually converge towards very similar asymptotic values. These will be denoted by a star in exponent (i.e. P_p^{c*} and P_C^{c*}). We have here:

$$P_p^{c*} \approx P_C^{c*} = 12.7 \text{ kPa} \tag{15}$$

The time to reach stability can be interpreted as the time necessary to loose memory of the initialisation state. A certain amount of time is therefore required to reach a physically consistent state. This is the behaviour of a statistically isotropic porous medium [46], however stability might not be met for more complex poral structure materials [44]. Comparing Fig.11 and Fig.15, it must be noticed that the capillary pressures P_p^c and P_C^c converge while the global saturation is not stable yet. This shows that interface-defined capillary pressure becomes here independent of both time and saturation. The results are in agreement with other recent works in which capillary pressure defined at the interface level tends to converge after a certain time. This reinforces the idea that capillary pressure, as defined here, can be considered as a function of the geometry and the interface properties only. Based on such a definition, it can be regarded as independent on the saturation. Consequently, considering an interfacial capillary pressure avoids the use of saturation-capillary pressure relationship which limits have been highlighted previously.

3.3 Statistical description of the flow front

A methodology to describe the flow front in terms of probability of presence has been described in Section 2.2.3. An example of distribution of flow front at a given time t is represented in Fig.16. The distribution can be modeled by a Gaussian law $\mathscr{N}(\mu, \sigma;\ t)$ as justified in Section 2.2.3. However, this trend is not necessarily clear in practice. Indeed, identifying precisely the flow front can be difficult [60, 61]. Attribution errors such as depicted in Fig.10 may lead to alter the observed distribution. Yet, such a modeling will be kept as a first approach.

The temporal evolution of the flow front distribution is represented in Fig.17. The mean value $\mu(t)$ shows a linear trend over time. The standard deviation $\sigma(t)$ starts to increase before being roughly stable around a value σ^*. From Fig.17, this asymptotic value is estimated at $\sigma^* = 5.6\bar{r}$.

4 Discussion

Results from the proposed upscaling procedure have been presented in the previous section. These have now to be compared to experimental observations or to other numerical studies.

4.1 Saturation

Analogous curves to those represented in Fig.11 can be found in the literature for similar boundary conditions [17, 18]. Even for different geometries and scales, as long as a flow rate is prescribed, the saturation increases linearly until reaching a plateau. Asymptotic saturation value S_L^{max} should also be compared to void content obtained in other study for similar Ca. However, most of the contributions on fibrous media set at an intermediate mesoscopic scale: a dual-scale medium is thus considered as the liquid phase flows within and around yarns (i.e. bundle of fibres) [16, 17, 58, 62, 63]. This work focuses more specifically on the fibre scale: only microvoids are studied here.

The fraction of residual vapor phase retrieved here is significantly higher than values commonly found in the literature. These generally lie between 1% and 10% for similar capillary numbers. It should be noticed that fibre fraction within yarns can reach really high values, around 75% [44]. For such a compacity, the fibrous arrangement tends towards a regular hexagonal packing. This entails an overall regular advancement of the flow front and thus a lower final void content. Moreover, further mechanisms such as air compressibility and dissolution [60] tend also to diminish the residual proportion of vapor phase. As regards local saturation, making a comparison with other studies can be complex. Indeed, most of them are located at a mesoscale involving a much larger saturation length. Here, the computed saturation length is around 25 μm for a mean fibre radius of 3.5 μm. Considering the directly upper scale on the order few millimeters [44], the scales seem to be well seperated. This means that at upper scales, the width of the unsaturated zone present at fibre scale can be neglected. In other terms, in 2D, the moving interface within the yarns can be wisely modeled by a 1D front in the equivalent homogeneous medium as it can be done with a level-set method.

4.2 Capillary pressure

A consistency between both methods to assess a resulting capillary pressure has been shown previously. Close asymptotic values are thus obtained and should be now compared to experimental results. Capillary pressure assessment in fibrous media has been a concern of the composite materials community over the past twenty years [7, 36, 63–65]. However, a huge dispersion of the results can be observed in practice as depicted in Fig.15. Therefore, the comparison of our results with those found in the literature can be a difficult task, especially because fibre volume ratio or the geometries can be different. However, the orders of magnitude remain consistent. Moreover, the mean value of the capillary pressure results found in the literature is 12.2 kPa. This value is very close to the asymptotic capillary pressure retrieved in this study (Eq.15). In addition, it seems appropriate to consider some of the presented experimental results as relevant bounds for capillary pressure. Considering Fig.15, results from [64] represents a relevant lower bound while Pucci *et al.* measurements [7] give a satisfactory upper bound.

Analytical models have been also established to assess capillary pressure within fibrous media [66–71]. The macroscopic contribution of capillary pressure is then expressed as:

$$P_c = \frac{\gamma_{SV} - \gamma_{SL}}{r} \frac{V_f}{1 - V_f} \tag{16}$$

where r is the fibre radius. For our material data and replacing r by the mean fibre radius $\bar{r}$, this equation (Eq.16) estimates the resulting capillary pressure at 8.2 kPa as represented in Fig.15. Even if this value is lower than ours, it provides a satisfactory estimation. Indeed, we are considering here a single random microstructure: a further statistical assessment of the capillary pressure should be performed. In addition, the stochasticity of the geometry under consideration (i.e. radius randomness, fibre position randomness,...) may alter the expression of Eq.16.

4.3 Statistical description of the flow front

In Section 3.3, the flow front distribution has been characterised by a Gaussian law. The advancement of distribution mean value has been shown to be linear over time for flow rate inlet control conditions. This is consistent with the saturation curve represented in Fig.11. We can thus write:

$$\mu(t) \propto S_L(t) \tag{17}$$

The standard deviation $\sigma(t)$ of the flow front distribution can be physically interpreted as a bandwidth within which the transient behaviour is contained.

This is very close to the concept of saturation length that has been introduced previously. It should be remarked that both ℓ_s and σ^* have comparable values. Seeing these quantities as characteric length for the transient behaviour, both approaches appear to be consistent. Once again, it can be concluded that the spread of the flow front can be neglected at upper scales. This may justify the use of deterministic approach at both mesoscale and macroscale. Moreover, this reaffirms the relevance of considering a sharp interface at upper scales. This conclusion directly depends on the kind of porous medium under consideration as well as the flow parameters such as the capillary number [25]. In a more general case, the tools presented here provide a detailed description of the flow and give a thorough upscaling procedure.

Finally, in the context of this work, results arising from saturation (Section 3.1) and from the consideration of a flow front distribution (Section 3.3) are in close agreement. As noticed previously, this latter technique requires the identification of the flow front which can be challeging in practice. As a result, it seems preferable to use saturation-based methods for similar porous media and flow settings.

4.4 SRVEs and statistical mechanical response

In Section 2.1.3, the microstructures under consideration have been qualified as Statistical Representative Volume Elements, following the results from a previous study [46] and the definition from [52]. Indeed, our geometries are randomly generated and have been found to provide both a mechanical and geometrical representativity. In other words, given the SRVE nature of the generated geometries, the mechanical response of a single microstructure will be representative of a whole family of other geometries generated with similar fibre ratio volume and with analoguous flow conditions.

To illustrate it, the response of six randomly generated volumes with V_f equal to 50% are presented in Fig.18 and Fig.19, for $Ca = 10^{-3}$. It can be seen that the responses are indeed very close, both in terms of saturation or capillary pressure, even if an intrinsic dispersion is naturally observed. Since the present work aims at demonstrating the basics of the stochastic upscaling methodology dedicated to transient flows in composites manufacturing, a single SRVE has been considered. Obviously, a more exhaustive study is requested to further investigate the statistical upscaled flows in the space of the physical and geometrical descriptors.

5 Conclusion

This work contributes to bridge the approaches developed by hydrogeology and composite materials communities in order to reach an upscaling method that is adapted to the impregnation of fibrous materials. From an in-depth analysis of the methods encountered in literature, a re-examination of the usual upscaling descriptors has been performed, so that they can relevantly characterise the imbibition of fibrous materials.

From 2D SRVEs, flow simulations have been performed through a stabilised finite element method. Upscaling methods have been then identified from the developments of various scientific communities. Those have been adapted to the context of random fibrous media at microscale and further strategies have been proposed.

First, the notion of saturation, that usually describes the proportion of liquid within the poral space, has been considered both at volume and section scales. Their temporal and/or spatial evolution naturally leads to upscaling descriptors related to saturation dynamics or void content. Results are consistent and the some identified discrepancies with the literature has been justified. Local saturation allows to determine a saturation length within which the transient behaviour is supposed to be contained. This length represents around 15% of the domain size. This allows us to conclude that the scales are well separated as the domain encompasses the entire transient behaviour. At upper scales, the width of the unsaturated zone may be neglected for the standard composite materials under consideration.

Then two methods have been proposed to assess a resulting capillary pressure from the interface behaviour. Both approaches have been validated on a test case and show an excellent agreement. A convergence of the capillary pressure is observed over time. It is thus independent of the saturation and only depends on the interface properties and inlet flow control. This may avoid the use of cumbersome relationship between saturation and capillary pressure. Our values of capillary pressure have been then shown to be in accordance with other analytical and experimental results.

A novelty of this approach is to describe the flow front through a statistical modelling. After identifying the position of the flow front, a presence distribution of the flow front is retrieved. In a first approach, this can be considered as a Gaussian law whose parameters behaviour are consistent with our proposed approach. In the situation under consideration, the spread parameter of the distribution is significantly lower than the characteristic length of the upper scale. This again jutifies deterministic modeling of the flow front at upper scales, for fibrous materials in the context of direct manufacting processes. However, in the case of larger anisotropic porous media, the distribution spread may not be negligible anymore and the proposed statistical characterisation may be particularly relevant.

Finally, the proposed strategy allows a thorough upscaling of the microscopic behaviour while justifying or reappraising some of the usual methods found in the literature. Both capillary number and fibre volume ratio has been kept constant here. Further studies should consider them as input variables of a more comprehensive model in which the presented upscaling descriptors are the output. This will allow to build a dataset so as to perform a more complete statistical characterisation of the upscaling.

This contribution focuses on the upscaling methods so as to retrieve a novel procedure that is suited for the impregnation of fibrous materials. The upscaling descriptors that have been highlighted are mostly scalar quantities and provide a thorough macroscopic characterisation of the flow under consideration. In future contributions, the influence of the flow settings and pore structure (*i.e.* Ca and V_f) on those descriptors will be investigated in order to extract constitutive laws ruling the imbibition of fibrous structures.

References

[1] Yan, G., Li, Z., Galindo Torres, S., Scheuermann, A., Li, L.: Transient Two-Phase Flow in Porous Media: A Literature Review and Engineering Application in Geotechnics. Geotechnics 2022, 2, 32–91 (2022)

[2] Whitaker, S.: Flow in porous media i: A theoretical derivation of darcy's law. Transport in porous media **1**(1), 3–25 (1986)

[3] Hassanizadeh, S.M., Gray, W.G.: Toward an improved description of the physics of two-phase flow. Advances in Water Resources **16**(1), 53–67 (1993)

[4] Michaud, V.: A review of non-saturated resin flow in liquid composite moulding processes. Transport in porous media **115**(3), 581–601 (2016)

[5] Bodaghi, M., Lomov, S., Simacek, P., Correia, N., Advani, S.: On the variability of permeability induced by reinforcement distortions and dual scale flow in liquid composite moulding: A review. Composites Part A: Applied Science and Manufacturing **120**, 188–210 (2019)

[6] Darcy, H.: Les fontaines publiques de la ville de dijon: exposition et application... (1856)

[7] Pucci, M.F., Liotier, P.-J., Drapier, S.: Capillary wicking in a fibrous reinforcement–orthotropic issues to determine the capillary pressure components. Composites Part A: Applied Science and Manufacturing **77**, 133–141 (2015)

[8] Teixidó, H., Staal, J., Caglar, B., Michaud, V.: Capillary effects in fiber reinforced polymer composite processing: A review. Front. Mater. 9: 809226. doi: 10.3389/fmats (2022)

[9] Kalaydjian, F.: A macroscopic description of multiphase flow in porous media involving spacetime evolution of fluid/fluid interface. Transport in Porous Media **2**(6), 537–552 (1987)

[10] Hassanizadeh, S.M., Gray, W.G.: Mechanics and thermodynamics of multiphase flow in porous media including interphase boundaries. Advances in water resources **13**(4), 169–186 (1990)

[11] Whitaker, S.: Flow in porous media ii: The governing equations for immiscible, two-phase flow. Transport in porous media **1**(2), 105–125 (1986)

[12] Ambekar, A.S., Mattey, P., Buwa, V.V.: Pore-resolved two-phase flow in

a pseudo-3d porous medium: Measurements and volume-of-fluid simulations. Chemical Engineering Science **230**, 116128 (2021)

[13] Kuentzer, N., Simacek, P., Advani, S.G., Walsh, S.: Correlation of void distribution to vartm manufacturing techniques. Composites Part A: applied science and manufacturing **38**(3), 802–813 (2007)

[14] Gopala, V.R., van Wachem, B.G.: Volume of fluid methods for immiscible-fluid and free-surface flows. Chemical Engineering Journal **141**(1-3), 204–221 (2008)

[15] Labat, L., Grisel, M., Breard, J., Bouquet, G.: Original use of electrical conductivity for void detection due to injection conditions of composite materials. Comptes Rendus de l'Académie des Sciences-Series IIB-Mechanics **329**(7), 529–534 (2001)

[16] Park, C.H., Lebel, A., Saouab, A., Bréard, J., Lee, W.I.: Modeling and simulation of voids and saturation in liquid composite molding processes. Composites Part A: Applied science and manufacturing **42**(6), 658–668 (2011)

[17] Villière, M., Guéroult, S., Sobotka, V., Boyard, N., Bréard, J., Delaunay, D.: Dynamic saturation curve measurement in liquid composite molding by heat transfer analysis. Composites Part A: Applied Science and Manufacturing **69**, 255–265 (2015)

[18] Gascón, L., García, J., LeBel, F., Ruiz, E., Trochu, F.: Numerical prediction of saturation in dual scale fibrous reinforcements during liquid composite molding. Composites Part A: Applied Science and Manufacturing **77**, 275–284 (2015)

[19] Nordlund, M., Michaud, V.: Dynamic saturation curve measurement for resin flow in glass fibre reinforcement. Composites Part A: Applied Science and Manufacturing **43**(3), 333–343 (2012)

[20] Fischer, R., Schlepütz, C.M., Hegemann, D., Rossi, R.M., Derome, D., Carmeliet, J.: Four-dimensional imaging and free-energy analysis of sudden pore-filling events in wicking of yarns. Physical Review E **103**(5), 053101 (2021)

[21] Hassanizadeh, S.M., Gray, W.G.: Thermodynamic basis of capillary pressure in porous media. Water resources research **29**(10), 3389–3405 (1993)

[22] Van Genuchten, M.T.: A closed-form equation for predicting the hydraulic conductivity of unsaturated soils. Soil science society of America journal **44**(5), 892–898 (1980)

[23] Hassanizadeh, S.M., Celia, M.A., Dahle, H.K.: Dynamic effect in the capillary pressure–saturation relationship and its impacts on unsaturated flow. Vadose Zone Journal **1**(1), 38–57 (2002)

[24] Armstrong, R.T., Porter, M.L., Wildenschild, D.: Linking pore-scale interfacial curvature to column-scale capillary pressure. Advances in Water resources **46**, 55–62 (2012)

[25] Ferrari, A., Lunati, I.: Direct numerical simulations of interface dynamics to link capillary pressure and total surface energy. Advances in water resources **57**, 19–31 (2013)

[26] Schlüter, S., Berg, S., Li, T., Vogel, H.-J., Wildenschild, D.: Time scales of relaxation dynamics during transient conditions in two-phase flow. Water

Resources Research **53**(6), 4709–4724 (2017)

[27] Camps-Roach, G., O'Carroll, D.M., Newson, T.A., Sakaki, T., Illangasekare, T.H.: Experimental investigation of dynamic effects in capillary pressure: Grain size dependency and upscaling. Water Resources Research **46**(8) (2010)

[28] Joekar-Niasar, V., Hassanizadeh, S.M.: Effect of fluids properties on non-equilibrium capillarity effects: Dynamic pore-network modeling. International Journal of Multiphase Flow **37**(2)

[29] Dahle, H.K., Celia, M.A., Majid Hassanizadeh, S.: Bundle-of-tubes model for calculating dynamic effects in the capillary-pressure-saturation relationship. Transport in Porous media **58**(1), 5–22 (2005)

[30] Cai, J.-C., Chen, Y., Qiao, J.-C., Yang, L., Zeng, J.-H., Sun, C.-H.: Determination of dynamic capillary effect on two-phase flow in porous media: A perspective from various methods. Petroleum Science (2022)

[31] Bottero, S., Hassanizadeh, S.M., Kleingeld, P.: From local measurements to an upscaled capillary pressure–saturation curve. Transport in Porous Media **88**(2), 271–291 (2011)

[32] Joekar-Niasar, V., Hassanizadeh, S.M., Dahle, H.: Non-equilibrium effects in capillarity and interfacial area in two-phase flow: dynamic pore-network modelling. Journal of Fluid Mechanics **655**, 38–71 (2010)

[33] Konangi, S., Palakurthi, N.K., Karadimitriou, N.K., Comer, K., Ghia, U.: Comparison of pore-scale capillary pressure to macroscale capillary pressure using direct numerical simulations of drainage under dynamic and quasi-static conditions. Advances in Water Resources **147**, 103792

(2021)

[34] Starnoni, M., Pokrajac, D.: On the concept of macroscopic capillary pressure in two-phase porous media flow. Advances in Water Resources **135**, 103487 (2020)

[35] Shokri, J., Godinez-Brizuela, O.E., Erfani, H., Chen, Y., Babaei, M., Berkowitz, B., Niasar, V.: Impact of displacement direction relative to heterogeneity on averaged capillary pressure-saturation curves. Water Resources Research **58**(2), 2021–030748 (2022)

[36] Willenbacher, B., May, D., Mitschang, P.: Out–of–plane capillary pressure of technical textiles. Composites Part A: Applied Science and Manufacturing **124**, 105495 (2019)

[37] Chevalier, L., Bruchon, J., Moulin, N., Liotier, P.-J., Drapier, S.: Accounting for local capillary effects in two-phase flows with relaxed surface tension formulation in enriched finite elements. Comptes Rendus Mécanique **346**(8), 617–633 (2018)

[38] Pucci, M.F., Liotier, P.-J., Drapier, S.: Tensiometric method to reliably assess wetting properties of single fibers with resins: Validation on cellulosic reinforcements for composites. Colloids and Surfaces A: Physicochemical and Engineering Aspects **512**, 26–33 (2017)

[39] Osher, S., Fedkiw, R.P.: Level set methods: an overview and some recent results. Journal of Computational physics **169**(2), 463–502 (2001)

[40] Shakoor, M., Scholtes, B., Bouchard, P.-O., Bernacki, M.: An efficient and parallel level set reinitialization method–application to micromechanics

and microstructural evolutions. Applied Mathematical Modelling **39**(23-24), 7291–7302 (2015)

[41] Min, C.: On reinitializing level set functions. Journal of computational physics **229**(8), 2764–2772 (2010)

[42] Blais, M., Moulin, N., Liotier, P.-J., Drapier, S.: Resin infusion-based processes simulation: coupled stokes-darcy flows in orthotropic preforms undergoing finite strain. International Journal of Material Forming **10**(1), 43–54 (2017)

[43] Chevalier, L.: Accounting for capillary effects in level-set based finite elements modelling of impregnation in fibrous media. PhD thesis, Université de Lyon (2019)

[44] Geoffre, A., Wielhorski, Y., Moulin, N., Bruchon, J., Drapier, S., Liotier, P.-J.: Influence of intra-yarn flows on whole 3d woven fabric numerical permeability: from stokes to stokes-darcy simulations. International Journal of Multiphase Flow **129**, 103349 (2020)

[45] Liu, Y., Moulin, N., Bruchon, J., Liotier, P.-J., Drapier, S.: Towards void formation and permeability predictions in lcm processes: a computational bifluid–solid mechanics framework dealing with capillarity and wetting issues. Comptes Rendus Mécanique **344**(4-5), 236–250 (2016)

[46] Geoffre, A., Ghestin, M., Moulin, N., Bruchon, J., Drapier, S.: Bounding transverse permeability of fibrous media: a statistical study from random representative volume elements with consideration of fluid slip. International Journal of Multiphase Flow **143**, 103751 (2021)

[47] Abouorm, L., Troian, R., Drapier, S., Bruchon, J., Moulin, N.: Stokes–darcy coupling in severe regimes using multiscale stabilisation for mixed finite elements: monolithic approach versus decoupled approach. European Journal of Computational Mechanics **23**(3-4), 113–137 (2014)

[48] Pacquaut, G., Bruchon, J., Moulin, N., Drapier, S.: Combining a level-set method and a mixed stabilized p1/p1 formulation for coupling stokes–darcy flows. International Journal for Numerical Methods in Fluids **69**(2), 459–480 (2012)

[49] Codina, R.: A stabilized finite element method for generalized stationary incompressible flows. Computer methods in applied mechanics and engineering **190**(20-21), 2681–2706 (2001)

[50] Hughes, T.J.: Multiscale phenomena: Green's functions, the dirichlet-to-neumann formulation, subgrid scale models, bubbles and the origins of stabilized methods. Computer methods in applied mechanics and engineering **127**(1-4), 387–401 (1995)

[51] Brooks, A.N., Hughes, T.J.: Streamline upwind/petrov-galerkin formulations for convection dominated flows with particular emphasis on the incompressible navier-stokes equations. Computer methods in applied mechanics and engineering **32**(1-3), 199–259 (1982)

[52] Trias, D., Costa, J., Turon, A., Hurtado, J.: Determination of the critical size of a statistical representative volume element (srve) for carbon reinforced polymers. Acta materialia **54**(13), 3471–3484 (2006)

[53] Kang, M.K., Lee, W.I., Hahn, H.T.: Formation of microvoids during resin-transfer molding process. Composites Science and Technology **60**(12-13),

2427–2434 (2000)

[54] Kunz, P., Zarikos, I., Karadimitriou, N., Huber, M., Nieken, U., Hassanizadeh, S.: Study of multi-phase flow in porous media: comparison of sph simulations with micro-model experiments. Transport in Porous Media **114**(2), 581–600 (2016)

[55] Rasmussen, C.E.: Gaussian processes in machine learning. In: Summer School on Machine Learning, pp. 63–71 (2003). Springer

[56] Trochu, F.: A contouring program based on dual kriging interpolation. Engineering with computers **9**(3), 160–177 (1993)

[57] Ausas, R.F., Buscaglia, G.C., Idelsohn, S.R.: A new enrichment space for the treatment of discontinuous pressures in multi-fluid flows. International Journal for Numerical Methods in Fluids **70**(7), 829–850 (2012)

[58] Leclerc, J.S., Ruiz, E.: Porosity reduction using optimized flow velocity in resin transfer molding. Composites Part A: Applied Science and Manufacturing **39**(12), 1859–1868 (2008)

[59] Ruiz, E., Achim, V., Soukane, S., Trochu, F., Bréard, J.: Optimization of injection flow rate to minimize micro/macro-voids formation in resin transfer molded composites. Composites science and technology **66**(3-4), 475–486 (2006)

[60] Park, C.H., Woo, L.: Modeling void formation and unsaturated flow in liquid composite molding processes: a survey and review. Journal of reinforced plastics and composites **30**(11), 957–977 (2011)

[61] Causse, P., Ravey, C., Trochu, F.: Capillary characterization of fibrous

reinforcement and optimization of injection strategy in resin transfer molding. Journal of Composites Science **2**(2), 19 (2018)

[62] DeValve, C., Pitchumani, R.: Simulation of void formation in liquid composite molding processes. Composites Part A: Applied Science and Manufacturing **51**, 22–32 (2013)

[63] Schell, J., Deleglise, M., Binetruy, C., Krawczak, P., Ermanni, P.: Numerical prediction and experimental characterisation of meso-scale-voids in liquid composite moulding. Composites Part A: applied science and manufacturing **38**(12), 2460–2470 (2007)

[64] Amico, S., Lekakou, C.: An experimental study of the permeability and capillary pressure in resin-transfer moulding. Composites Science and Technology **61**(13), 1945–1959 (2001)

[65] Koubaa, S., Burtin, C., Le Corre, S.: Investigation of capillary impregnation for permeability prediction of fibrous reinforcements. Journal of Composite Materials **50**(11), 1417–1429 (2016)

[66] Vilà, J., Sket, F., Wilde, F., Requena, G., González, C., LLorca, J.: An in situ investigation of microscopic infusion and void transport during vacuum-assisted infiltration by means of x-ray computed tomography. Composites science and technology **119**, 12–19 (2015)

[67] Pillai, K.M., Advani, S.G.: Wicking across a fiber-bank. Journal of colloid and interface science **183**(1), 100–110 (1996)

[68] Bayramli, E., Powell, R.: The normal (transverse) impregnation of liquids into axially oriented fiber bundles. Journal of colloid and interface science **138**(2), 346–353 (1990)

[69] Neacsu, V., Obaid, A.A., Advani, S.: Spontaneous radial capillary impregnation across a bank of aligned micro-cylinders–part i: Theory and model development. International journal of multiphase flow **32**(6), 661–676 (2006)

[70] Ahn, K., Seferis, J., Berg, J.: Simultaneous measurements of permeability and capillary pressure of thermosetting matrices in woven fabric reinforcements. Polymer composites **12**(3), 146–152 (1991)

[71] Yeager, M., Hwang, W.R., Advani, S.G.: Prediction of capillary pressure for resin flow between fibers. Composites Science and Technology **126**, 130–138 (2016)

Statements and Declarations

The authors declare that no funds, grants, or other support were received during the preparation of this manuscript. The authors have no relevant financial or non-financial interests to disclose.

γ_{SV} (N/mm)	γ_{SL} (N/mm)	γ_{LV} (N/mm)	η_V (Pa.s)	η_L (Pa.s)
54.7×10^{-3}	25.9×10^{-3}	50.8×10^{-3}	1.71×10^{-5}	2.76×10^{-3}

Table 1: Fluid properties chosen for the numerical simulations.

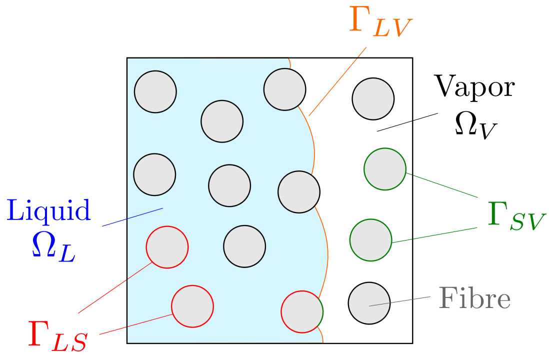

Figure 1: Imbibition in a fibrous medium: domains, boundaries and notations.

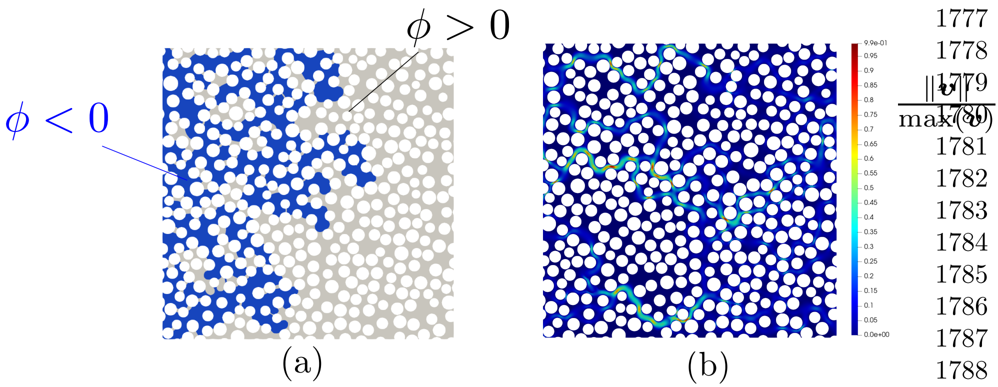

Figure 2: A simulation example of transient two-phase flow within a generated fibrous microstructure: (a) location of the phases (blue: liquid, grey: vapor), (b) normalised velocity magnitude.

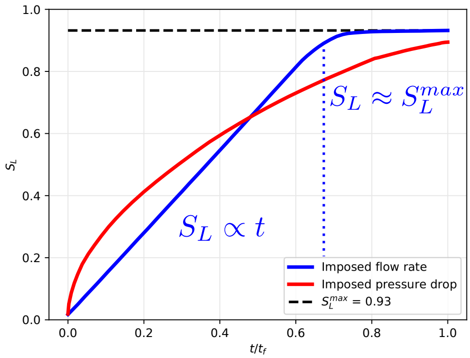

Figure 3: Temporal evolution of global saturation S_L for different inlet boundary conditions.

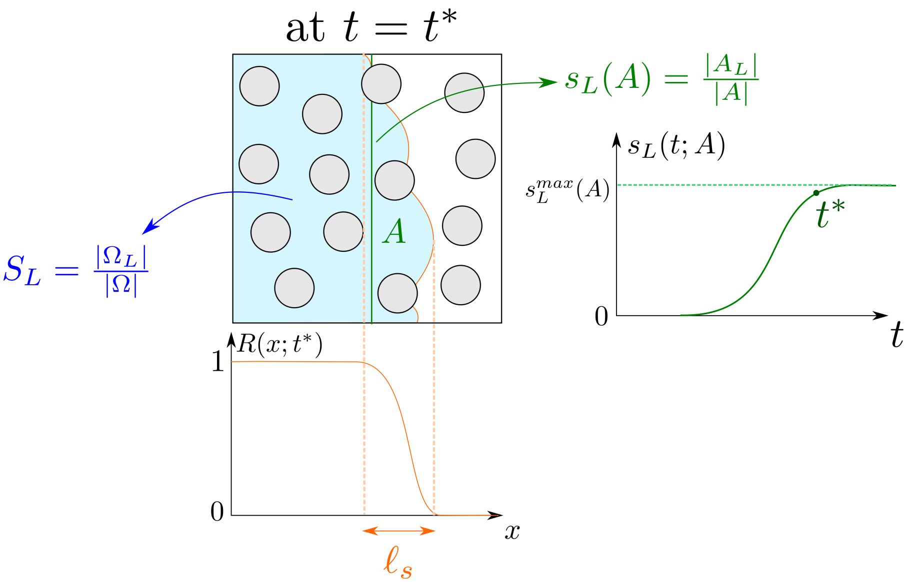

Figure 4: Notions of saturation and saturation length.

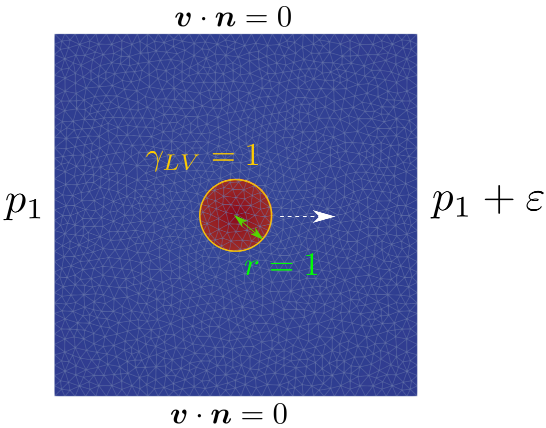

Figure 5: Test case for the validation of the resulting capillary pressure computation : parameters, boundary conditions and mesh (1655 nodes). A pressure drop of low intensity ε is prescribed.

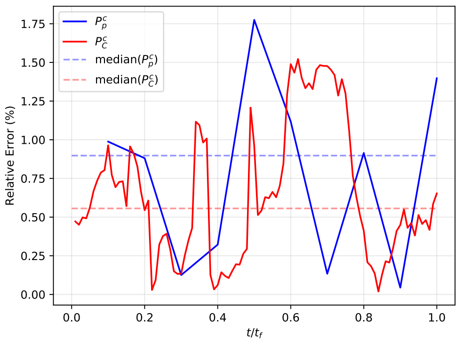

Figure 6: Relative error between reference value and the two methods to assess the resulting capillary pressure for a given mesh (1215 nodes).

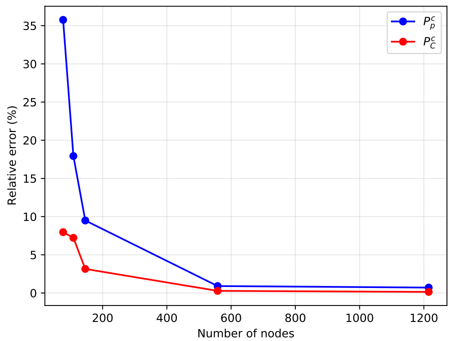

Figure 7: Mesh convergence for the two methods to assess the resulting capillary pressure.

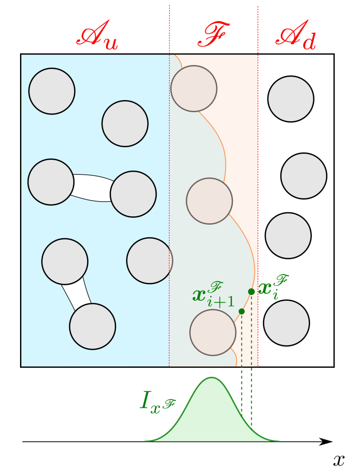

Figure 8: Statistical approach to describe the flow front.

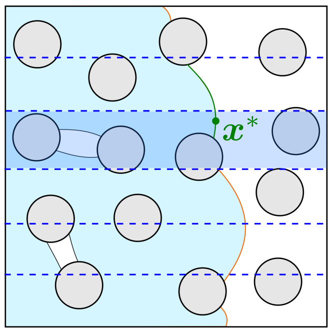

Figure 9: A method to identify the flow front.

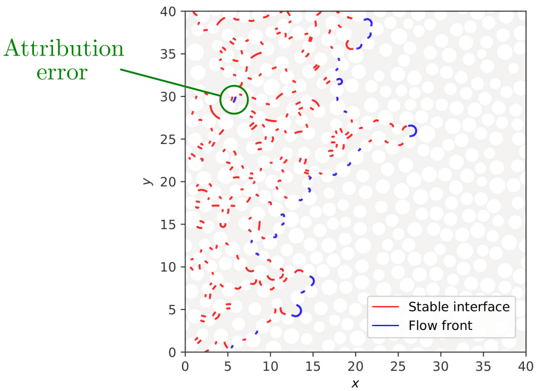

Figure 10: Example of flow front identification.

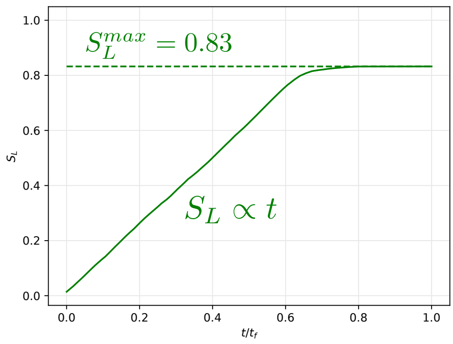

Figure 11: Temporal evolution of the global saturation.

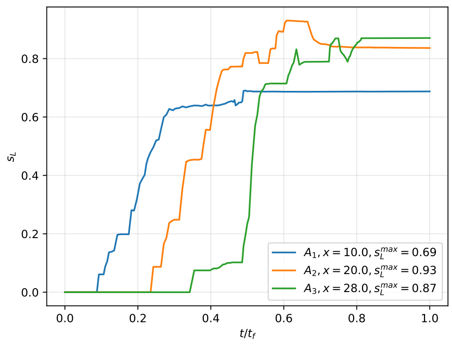

Figure 12: Temporal evolution of the saturation of three sections characterised by their abscissa x.

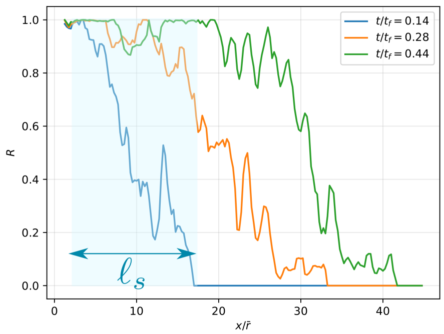

Figure 13: Spatial evolution of the ratio R for three given times.

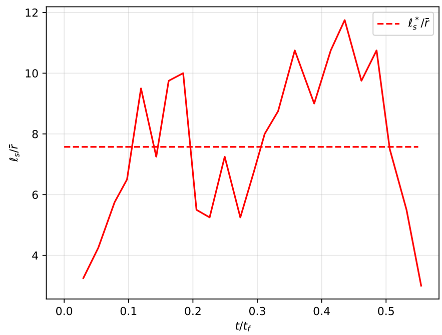

Figure 14: Temporal evolution of the saturation length normalised by the mean fibre radius.

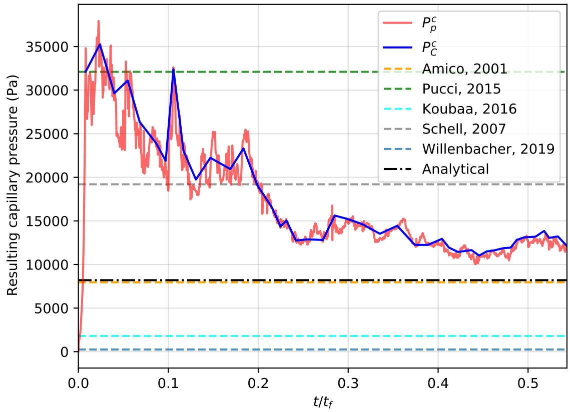

Figure 15: Temporal evolution of the resulting capillary pressure defined at the interface level: proposed methods and literature.

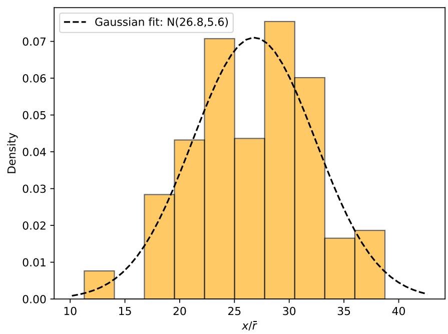

Figure 16: Distribution of flow front at $t/t_f = 0.73$.

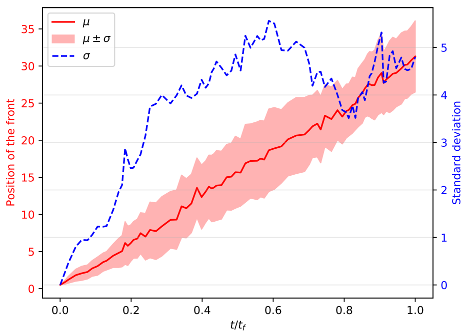

Figure 17: Distribution of flow front over time: mean value, dispersion and standard deviation.

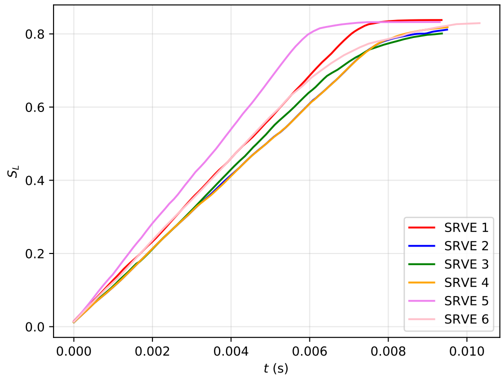

Figure 18: Time evolution of the global saturation for six randomly generated microstructures ($V_f = 50\%$, $Ca = 10^{-3}$).

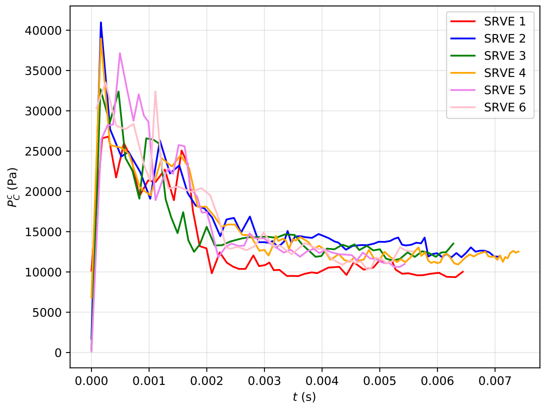

Figure 19: Time evolution of the resulting capillary pressure for six randomly generated microstructures ($V_f = 50\%$, $Ca = 10^{-3}$).